TU Delft

Delft University of Technology

Understanding the role of air and protein phase on mechanical anisotropy of calcium caseinate fibers

Wang, Zhaojun; Tian, Bei; Boom, Remko; van der Goot, Atze Jan

DOI
10.1016/j.foodres.2019.01.009

Publication date
2019

Document Version
Final published version

Published in
Food Research International

Citation (APA)
Wang, Z., Tian, B., Boom, R., & van der Goot, A. J. (2019). Understanding the role of air and protein phase on mechanical anisotropy of calcium caseinate fibers. *Food Research International*, *121*, 862-869. https://doi.org/10.1016/j.foodres.2019.01.009

Important note
To cite this publication, please use the final published version (if applicable).
Please check the document version above.

Copyright
Other than for strictly personal use, it is not permitted to download, forward or distribute the text or part of it, without the consent of the author(s) and/or copyright holder(s), unless the work is under an open content license such as Creative Commons.

Takedown policy
Please contact us and provide details if you believe this document breaches copyrights.
We will remove access to the work immediately and investigate your claim.

This work is downloaded from Delft University of Technology.
For technical reasons the number of authors shown on this cover page is limited to a maximum of 10.

Food Research International 121 (2019) 862–869

Contents lists available at ScienceDirect

Food Research International

journal homepage: www.elsevier.com/locate/foodres

Understanding the role of air and protein phase on mechanical anisotropy of calcium caseinate fibers

Zhaojun Wang[a], Bei Tian[b], Remko Boom[a], Atze Jan van der Goot[a,*]

[a] Food Process Engineering, Wageningen University & Research, PO Box 17, 6700AA Wageningen, the Netherlands
[b] Department of Radiation Science and Technology, Faculty of Applied Science, Delft University of Technology, Mekelweg 15, 2629JB Delft, the Netherlands

ARTICLE INFO

Keywords:
Air bubbles
Calcium caseinate
Fibers
Mechanical property
Anisotropy
Shear

ABSTRACT

Calcium caseinate dispersions can be transformed into anisotropic, fibrous materials using the concept of shear-induced structuring. The aim of this study is to further investigate the relative importance of air bubbles and protein on the mechanical anisotropy of calcium caseinate material. In this study, the effect of air on mechanical anisotropy of these fibrous materials was described with a load-bearing model, with the void fraction, and the bubble length and width as input parameters. The anisotropy of the protein phase was estimated using materials obtained from deaerated dispersions after shearing at different shear rates. We concluded that the deformation of air bubbles can only partly explain the mechanical anisotropy; the anisotropy of the protein phase is more important. Based on all results, we further concluded that the anisotropy of the protein phase was affected by the air bubbles present during the structuring process. This effect was explained by locally higher shear rate in the protein matrix during the structuring process.

1. Introduction

Dense calcium caseinate dispersions have been successfully transformed into a hierarchically fibrous structure using a process based on simple shear flow deformation (Manski, van der Goot, & Boom, 2007). Such fibrous material is structural and mechanical anisotropy. The presence of a pronounced fibrous structure is crucial for the development of an appealing meat analog in terms of acceptability of consumers (Hoek et al., 2011). Therefore, calcium caseinate becomes an attractive material for the next generation of meat analogs.

The formation of calcium caseinate fibrous structure is based on the presence of caseinate micelles (~100–200 nm) in the dispersion. Further, these micelles exhibit mild adhesion due to the divalent calcium ions (Manski, van der Goot, and Boom, 2007; Manski, van Riemsdijk, Boom, & van der Goot, 2007). Upon shearing, those mildly adhesive micelles are aligned and concurrently fixated using transglutaminase. Recently, we found that the fibrous appearance and mechanical anisotropy of calcium caseinate materials are greatly enhanced by the presence of dispersed air bubbles (~100–400 μm) (Tian, Wang, van der Goot, & Bouwman, 2018; Wang, Tian, Boom, & van der Goot, 2019). Several studies have showed that the geometrical anisotropy of air bubbles could result in the mechanical anisotropy of aerated materials (Cho & Rizvi, 2009; Griffiths, Heap, Xu, Chen, & Baud, 2017; Hyun, Murakami, & Nakajima, 2001; Masmoudi et al., 2017; Nakajima, 2007). Therefore, it is interesting to quantify the effect of air bubbles on the mechanical anisotropy in calcium caseinate materials.

From a macroscopic viewpoint, the calcium caseinate fibrous material can be considered as a special foam in which air bubbles are dispersed within anisotropic protein matrices. Several empirical and theoretical models have been developed to predict the tensile properties of porous materials (Chen, Wu, & Zhou, 2013; Gibson & Ashby, 1997; Ji, Gu, & Xia, 2006; Rice, 1996b). Some of these models relate not only to total void fraction but also to the void geometry. For example, the load-bearing model is easily applied to idealized arrays of identically shaped and orientated voids (Rice, 1993). The load-bearing model assumes that the mechanical properties are determined by the minimum solid cross-sectional area parallel to the stress. In this approach, microstructural stress concentration effects are neglected (Rice, 1996a). Hyun et al. (2001) showed that load-bearing model is suitable to determine the strength of porous copper. Recently, a model based on the cross-sectional area of a weak dispersed phase was modified to predict mechanical anisotropy of the fibrous soy protein isolate-pectin material (Dekkers, Hamoen, Boom, & van der Goot, 2018).

In this study, we hypothesize that both the deformation of air and anisotropy of protein phase contribute to the macroscopic mechanical anisotropy. We apply the load-bearing model to quantify the effect of

* Corresponding author.
E-mail addresses: zhaojun.wang@wur.nl (Z. Wang), B.Tian-1@tudelft.nl (B. Tian), remko.boom@wur.nl (R. Boom), atzejan.vandergoot@wur.nl (A.J. van der Goot).

https://doi.org/10.1016/j.foodres.2019.01.009
Received 5 October 2018; Received in revised form 18 December 2018; Accepted 6 January 2019
Available online 10 January 2019
0963-9969/ © 2019 The Author(s). Published by Elsevier Ltd. This is an open access article under the CC BY-NC-ND license (http://creativecommons.org/licenses/BY-NC-ND/4.0/).

air in the calcium caseinate materials on their fracture properties. Both total void fraction and bubble geometry are considered. Fibrous materials were then prepared from aerated and from deaerated calcium caseinate dispersions using different shearing rates. Deaeration in these concentrated dispersions was achieved by heating, centrifuging and application of a long rehydration time before shearing (Wang et al., 2019). The geometry of the air bubbles in the final products was studied with X-ray tomography, while the directional tensile strengths were determined using a texture analyzer. Finally, the predicted mechanical anisotropy from the load-bearing model was compared to the mechanical anisotropy found experimentally.

2. Material and methods

2.1. Material

Spray dried calcium caseinate was kindly provided by DMV International (Veghel, the Netherlands). This calcium caseinate contained 92 wt% protein and 1.46 wt% calcium according to the manufacturer's specifications. The dry matter was 94.82 wt%. Weight was given as powder weight.

2.2. Protein dispersions preparation for preparative shearing

An aerated protein dispersion was prepared by manually mixing 30 wt% calcium caseinate powder in demineralized water (pH 6.7–6.9) with a spatula for 1 min. Deaeration was achieved through heating the dispersion at 80 °C for 5 min, followed by centrifuging (2500 ×*g* for 2 min) and subsequently leaving it at room temperature for 55 min.

2.3. Material preparation in the shear cell device

Well-defined shear flow was applied using a custom built shearing device (Wageningen University, the Netherlands), which consists of a rotating plate (the bottom cone, angle $\alpha_{plate} = 105^{\circ}$) and a stationary cone (the top cone, angle $\alpha_{cone} = 100^{\circ}$). Further details are described in an earlier publication (van der Zalm, Berghout, van der Goot, & Boom, 2012). The cones were temperature controlled with a heating and a cooling water bath. After preparation, the dispersion was immediately transferred to the pre-heated (50 °C) device. Dispersions were then subjected to shearing at various rates (0, 3, 10, 25, 50, 75, 100 or 150 rpm) for 5 min. After processing, the material was cooled for 10 min at 4 °C. Tensile tests were performed within 1 h after removing the sample from the shear cell device. Part of the materials was stored at −20 °C prior to further analysis. The preliminary results when using shear rates higher than 150 rpm were shown to be not reliable due to the instability of the inner cone during shearing.

2.4. Tensile strength analysis

A Texture Analyzer (Instron Testing System, table model type 5564) was used with a load cell of 100 N. The material that was not sheared (referred to as 0 rpm) was too weak to measure its tensile strength. From the other materials, dog-bone-shaped pieces were cut with a length of 15.2 mm and a width of 3.18 mm using a tensile bar. The thickness of the samples varied between 4 and 6 mm. The samples were taken parallel and perpendicular to the shear flow (based on the shear-vorticity plane). The tensile tests were conducted at a constant deformation speed of 3 mm s^{-1}. Grips with abrasive paper were used to prevent slip during testing. At least three specimens per direction were measured per sample, and three samples per condition were tested. The results obtained from these tensile tests were depicted as force-displacement curves. Blue Hill software was used to determine a fracture point and to calculate the fracture stress (σ, kPa) and fracture strain (ε, −).The ratio of the mechanical properties between the parallel and perpendicular directions to the shear flow was used as an index for the mechanical anisotropy of the samples.

2.5. X-ray tomography

Samples (roughly (3 ×4 ×20 mm) were scanned using a GE Phoenix v|tome|x m tomographer (General Electric, Wunstorf, Germany) set at 80 kV/90 μA. The system contains two X-ray sources; the 240 kV micro-focus tube with a tungsten target was used. The images were recorded by a GE DXR detector array with 2024 × 2024 pixels (pixel size, 200 μm). The detector and object were located 815 mm and 28.55 mm from the X-ray source, respectively. This results in a spatial resolution of 7.00 μm. A full scan consisted of 750 projections over 360°. Four images were taken for each projection. The first image was skipped because it probably contained information from the previous projection; images 2–4 were averaged into one projection. GE reconstruction software (Wunstorf, Germany) was used to calculate the 3D structure via back projection. The 3D images were analyzed using Avizo imaging software version 9.3.0. The analysis included the total volume, total air volume in the sample, void fraction of air (p), the length of air bubble parallel to the shear flow (a) and the average width of the air bubble perpendicular to the shear flow (b, based on velocity gradient-shear flow plane and vorticity-shear flow plane).

2.6. Reflective light microscopy

A fresh sample (50 rpm) was stretched by hands in the parallel direction to shear flow. The resulting deformed material was then observed with a digital microscope (Smartzoom 5) with 50× magnification.

3. Theory

Based on load-bearing model, the tensile stress of porous material is given as follows:

$$\sigma = \sigma_c \bullet \varphi \tag{1}$$

Where σ_c is the theoretical fracture stress in the same material without air; φ is the minimum cross-sectional area fraction of continuous phase. We simplify calcium caseinate material by considering the dispersed air bubbles as many small cubes inside a larger cube (h) (Fig. 1). We assume that all these cubes have a similar size and are deformed in a similar manner. The deformation will result in one dimension becoming longer (a), and we assume that the volume remains constant, and the two other dimensions will remain the same (b). Then,

$$p = \frac{a \bullet b^2}{h^3} \tag{2}$$

When stretching the material in the parallel direction of the shear flow (Fig. 1A), the minimum cross-sectional area fraction of the air bubbles is given by:

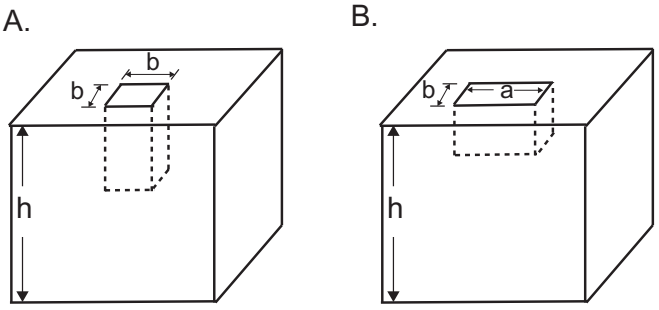

Fig. 1. Schematic of the load-bearing area model for calcium caseinate material with cuboid void: A) deformation (shear flow) direction parallel to the tensile stress; B) deformation (shear flow) direction perpendicular to the tensile stress.

$$\varphi_{\parallel} = 1 - \frac{b^2}{h^2} = 1 - \left(\frac{a}{b}\right)^{-\frac{2}{3}} \bullet p^{\frac{2}{3}} \quad (3)$$

When stretching the material in the perpendicular direction of the shear flow (Fig. 1B), the minimum cross-sectional area fraction of the air bubbles is given by:

$$\varphi_{\perp} = 1 - \frac{a \bullet b}{h^2} = 1 - \left(\frac{a}{b}\right)^{\frac{1}{3}} \bullet p^{\frac{2}{3}} \quad (4)$$

Combining Eqs. (3) and (4) into Eq. (1) yields:

$$\sigma_{\parallel} = \sigma_{c\parallel} \bullet \left(1 - \left(\frac{a}{b}\right)^{-\frac{2}{3}} \bullet p^{\frac{2}{3}}\right) \quad (5)$$

$$\sigma_{\perp} = \sigma_{c\perp} \bullet \left(1 - \left(\frac{a}{b}\right)^{\frac{1}{3}} \bullet p^{\frac{2}{3}}\right) \quad (6)$$

It should be noted that the values of $\sigma_{c\perp}$ and $\sigma_{c\parallel}$ are only the same in a matrix that is homogeneous (i.e. isotropic). In our case, the matrix consists of sheared calcium caseinate, which might be anisotropic. This explains why different symbols were taken to include anisotropy effect in Eq. (5)–(6).

We define the ratio between the fracture stress in the parallel and perpendicular directions as the anisotropy index (*AI*), which can be expressed as

$$AI = \frac{\sigma_{\parallel}}{\sigma_{\perp}} = \frac{\sigma_{c\parallel}}{\sigma_{c\perp}} \bullet \frac{1 - \left(\frac{a}{b}\right)^{-\frac{2}{3}} \bullet p^{\frac{2}{3}}}{1 - \left(\frac{a}{b}\right)^{\frac{1}{3}} \bullet p^{\frac{2}{3}}} = AI_{protein} \bullet AI_{air} \quad (7)$$

Thus, the anisotropy index of fracture stress *AI* is equal to the product of the anisotropy index of continuous phase $AI_{protein}$ and the anisotropy index of the deformed air bubble AI_{air}.

Fig. 2A demonstrates the effect of air holdup according to this model on the tensile stress in two directions, given a constant void fraction ($p = 0.2$) and assuming an isotropic continuous phase ($\sigma_{c\parallel} = \sigma_{c\perp} = 100\ kPa$). The fracture stress increases in the parallel direction with increased deformation of the air bubbles, and it decreases in the perpendicular direction. Consequently, the values of *AI* increases with increased deformation of the air bubbles. When it is assumed that the continuous phase is anisotropic ($\sigma_{c\parallel} = 100\ kPa; \sigma_{c\perp} = 50\ kPa$), the value of *AI* is twice compared to the material with an isotropic continuous phase. The *AI* can thus result from a combination of anisotropic protein phase and anisotropy originating from deformed air bubbles.

4. Results

4.1. Structure formation from aerated calcium caseinate

Aerated calcium caseinate dispersions (around 20.0 v% of air), were sheared at different shear rates (0–150 rpm, 5 min). Visual inspection of the resulting materials revealed clear differences. Without shear (0 rpm), the material was a weak, homogeneous gel without fibers or layers. The material that was sheared at 3 rpm was weak and easily broken when discharged from the device (Fig. 3A.). This material was anisotropic but did not contain fibers. The applications of a shear rate of 10 rpm or 25 rpm resulted in some thick fibers upon tearing the materials manually. Further increasing the shear rate to 50, 75 and 100 rpm resulted in pronounced fibrous materials (Fig. 3B). The material made at 150 rpm showed less fibers upon tearing compared to the material sheared at 50, 75 and 100 rpm.

The geometries of the aerated and sheared materials (Fig. 4) were analyzed using 2D and reconstructed 3D X-ray tomography (XRT). Without shearing (0 rpm), the air was randomly distributed throughout the protein matrix. Shearing calcium caseinate dispersion at 3 rpm resulted in slightly deformed air bubbles. This deformation increased with increasing shear rate, while the total air holdup clearly decreased when sheared at 150 rpm. In the latter material, the air was mostly located near the inner or stationary cone (left side of the 2D image), and only small air bubbles remained closer to the rotating outer cone (right side of the 2D image). This suggests that the larger air bubbles were expelled from the rotating outer cone during shear.

Shearing at different rates (0–150 rpm) affected both the total air holdup and the deformation of the air bubbles in the material (Fig. 5). Without shearing (0 rpm), the material contained 20.0 v% air, while visual observations showed hardly any bubble deformation. Fig. 5A shows that shearing reduced the total air holdup (variation between 13.6 and 15.1 v%) up to a shear rate of 25 rpm, which was mainly due to the loss of the smallest ($< 10^{-3}\ mm^3$) and the largest air bubbles ($> 10^{-1}\ mm^3$). The material sheared at 50 rpm contained the highest void fraction of 17.5 v% air among the sheared materials (but still lower than the material without shearing). At higher shear rates (75–150 rpm), the materials contained less air. Fig. 5B shows that the shear deforms air bubbles when their volumes are larger than $10^{-3}\ mm^3$. However the deformation did not strongly change when varying the shear rate between 3 and 75 rpm. The large air bubbles ($> 10^{-1}\ mm^3$) were mostly deformed when processing at 100 and 150 rpm. It is possible that shear force had an influence on the external forces that are resulting in deformation, breakup and coalescence of air bubbles. To summarize, overall air holdup decreased with higher shear rates, whereas the deformation degree of air bubbles was not strongly influenced by the shear rate.

Fig. 6 summarizes the effect of shear rate on the fracture mechanics of the materials. In the absence of shear, the material was too weak to perform a tensile test. The fracture stress and strain increased with increasing shear rate (3–75 rpm) in the parallel direction. Shearing at 3 rpm resulted in only slight anisotropy. Shearing at 10 and 25 rpm resulted in more pronounced anisotropy. These materials had a higher fracture stress parallel to the shear flow, and a lower fracture stress perpendicular to the shear flow when compared to the material that was sheared at 3 rpm. Materials sheared at 50, 75 and 100 rpm had most pronounced anisotropy. Their fracture stress and strain were the

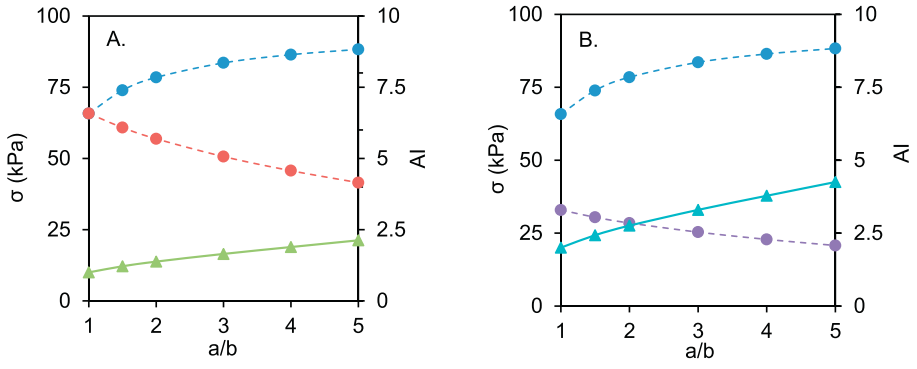

Fig. 2. (A) Calculation of the fracture stress in the parallel (●) and perpendicular (●) direction and anisotropy index *AI* (▲), while keeping a constant porosity ($p = 0.2$) and assuming an isotropic continuous phase ($\sigma_{c\parallel} = \sigma_{c\perp} = 100\ kPa$); (B) calculation of fracture stress in the parallel (●) and perpendicular (●) direction and anisotropy index *AI* (▲), while keeping a constant porosity ($p = 0.2$) and assuming an anisotropic continuous phase ($\sigma_{c\parallel} = 100\ kPa; \sigma_{c\perp} = 50\ kPa$). The lines have been added to guide the eye.

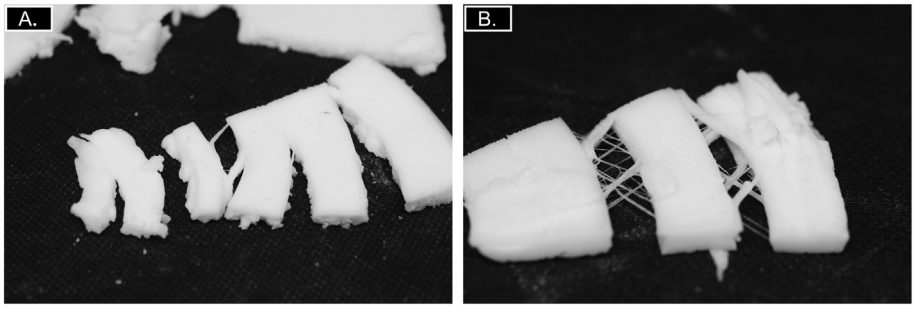

Fig. 3. Macrostructure of 30% aerated calcium caseinate material sheared at 3 rpm (A) and 75 rpm (B). The length of images is approximately 4–7 cm.

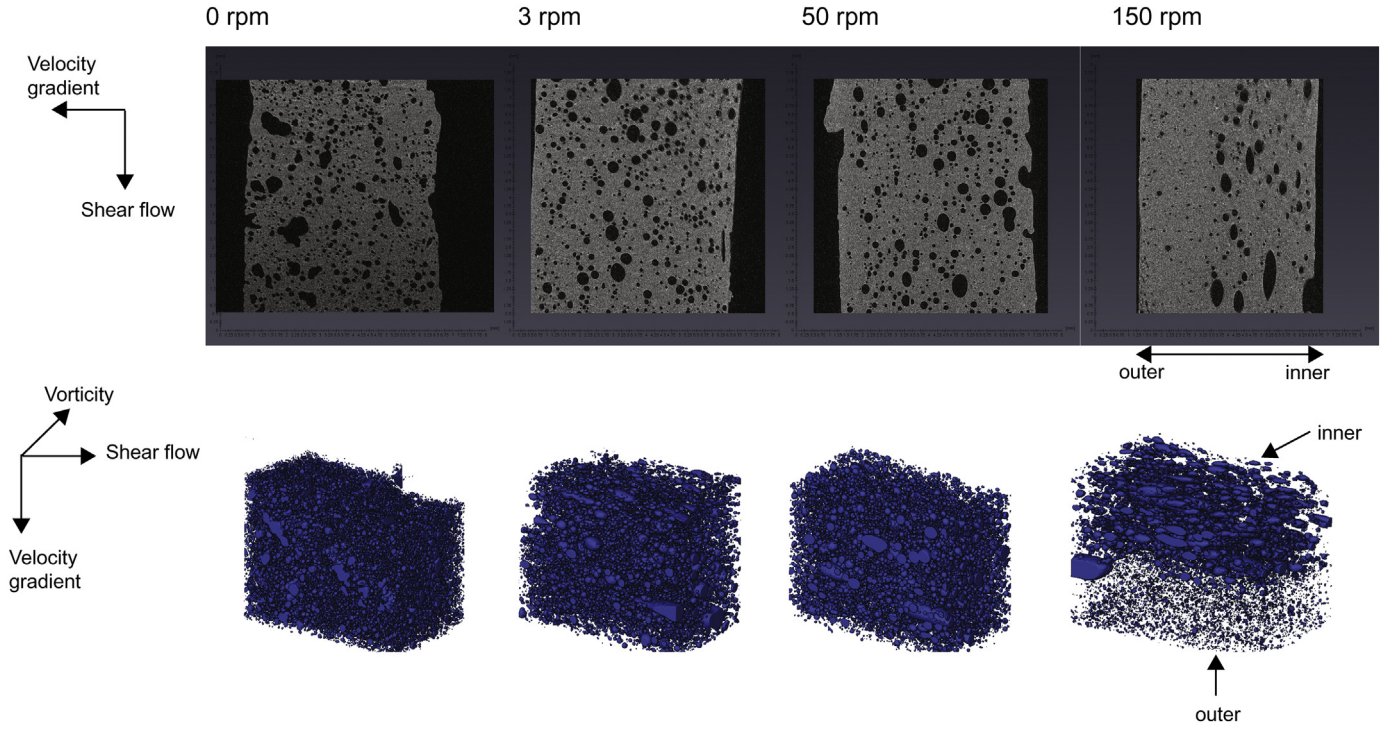

Fig. 4. X-ray tomography images of air bubbles in calcium caseinate material that were sheared at various shear rates (0, 3, 50 and 150 rpm) for 5 min.

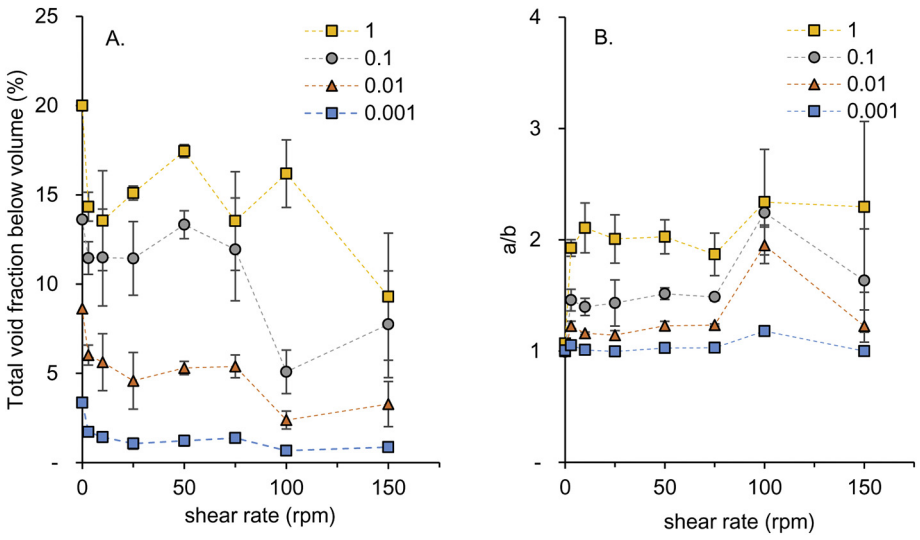

Fig. 5. X-Ray tomography analysis of air bubbles when varying the shear rate for 30% calcium caseinate materials: (A) overall void fraction and the void fraction at different volume ranges; (B) the ratio between long and short axis of the air bubbles (a/b) at different volume ranges. The error bars are ± standard deviation; where not visible, error bars were smaller than the marker used.

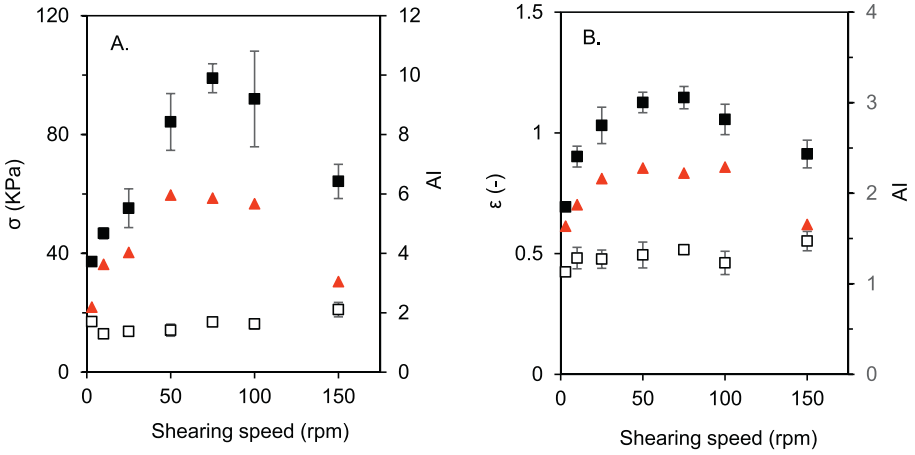

Fig. 6. Measured mechanical properties: (A) fracture stress σ and fracture strain ε (B) of 30% calcium caseinate materials as a function of shear rate (3, 10, 25, 50, 75, 100 and 150 rpm) parallel (■) and perpendicular (□) to the shear direction. The error bars are ± standard deviation; where not visible, error bars were smaller than the marker used. The anisotropy index (▲) is the ratio between the mechanical properties measured in the parallel and perpendicular directions.

highest in the parallel direction. The slight increase of the fracture stress in the perpendicular direction from 50 to 150 rpm can be explained by the decreasing of the air holdup. The material sheared at 150 rpm was much weaker compared to the materials sheared at 50–100 rpm in the parallel direction. The explanation could be that a high shear rate leads to break up the protein alignment.

4.2. Structure formation from deaerated calcium caseinate dispersions

In the absence of air bubbles, the 30 wt% calcium caseinate dispersions formed materials with different properties. Shearing at low rates (3, 10 and 25 rpm) resulted in isotropic materials accompanied by some expelled water and subtle syneresis (Fig. 7A). Further, the applied shear rates were too low to create anisotropy (Manski, van der Zalm, van der Goot, & Boom, 2008). Materials with an anisotropic structure were formed at higher shear rates (40–75 rpm). A further increase of the shear rate (100–150 rpm) resulted in fibers that were only visible upon tearing manually. Fig. 7C showed that the anisotropy index of fracture stress increased with increasing shear rate (40–150 rpm). A linear relationship was observed between the anisotropy index of fracture stress and shear rate with an intercept of 1 and a 95% confidence interval from 0.0248 to 0.0290. This empirical equation in Fig. 7C can be used to estimate the "theoretical" mechanical anisotropy index of the deaerated dispersions sheared at low rates (3–25 rpm).

5. Discussion

The sheared calcium caseinate materials are known to create an anisotropic structure. However, we identified the importance of an additional phase that also contributes to the material properties: the air phase (Wang et al., 2019). The importance of air is based on the large differences in the structural and mechanical anisotropy between the aerated and non-aerated materials, and the slight deformation of the air bubbles. However, anisotropy was also observed in the non-aerated materials, which means that the protein phase itself can become anisotropic as well. We therefore propose that both the protein matrix and the dispersed air bubbles contribute to the mechanical anisotropy in the material.

The X-ray tomography measurements provide the parameters needed to describe the change in mechanical properties due to the presence of air bubbles using the model. Those parameters are the volume fraction of the air p, the average length of the bubbles (a) parallel to the shear and the average width (b) perpendicular to the shear direction. With that, we calculate the fracture stress in the parallel ($\sigma_{\parallel}$) and the perpendicular ($\sigma_{\perp}$) directions as well as the anisotropy index (AI_{air}) of the fracture stress using Eq. (5)–(7).

One should bear in mind that the material will be extended during the tensile test in the parallel direction. This extension of the material in the direction of the shear flow will also extend the bubble (Fig. 8). To

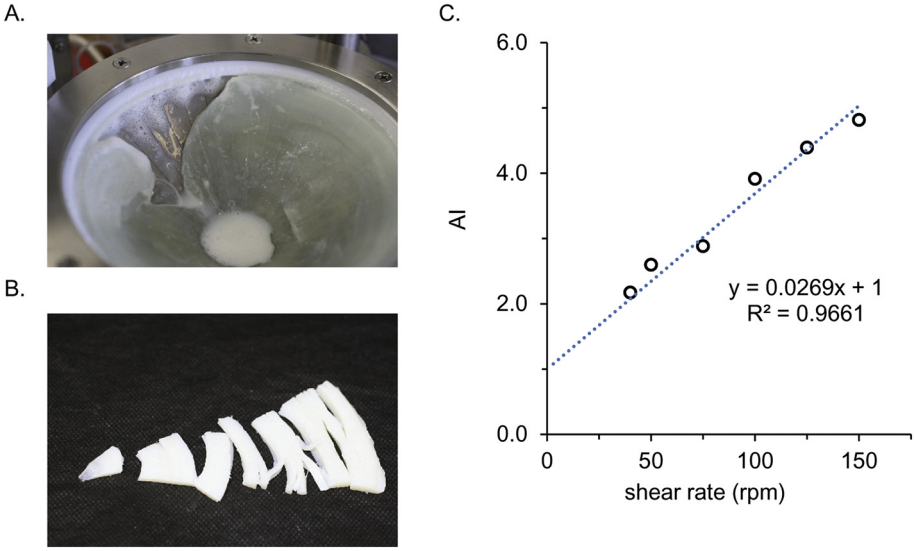

Fig. 7. Macrostructure of 30% deaerated calcium caseinate material sheared at 3 rpm (A) and 100 rpm (B). Anisotropy index of fracture stress for 30% deaerated calcium caseinate materials as a function of shear rate (40, 50, 75, 100,125 and 150 rpm). The dotted line represents the fit.

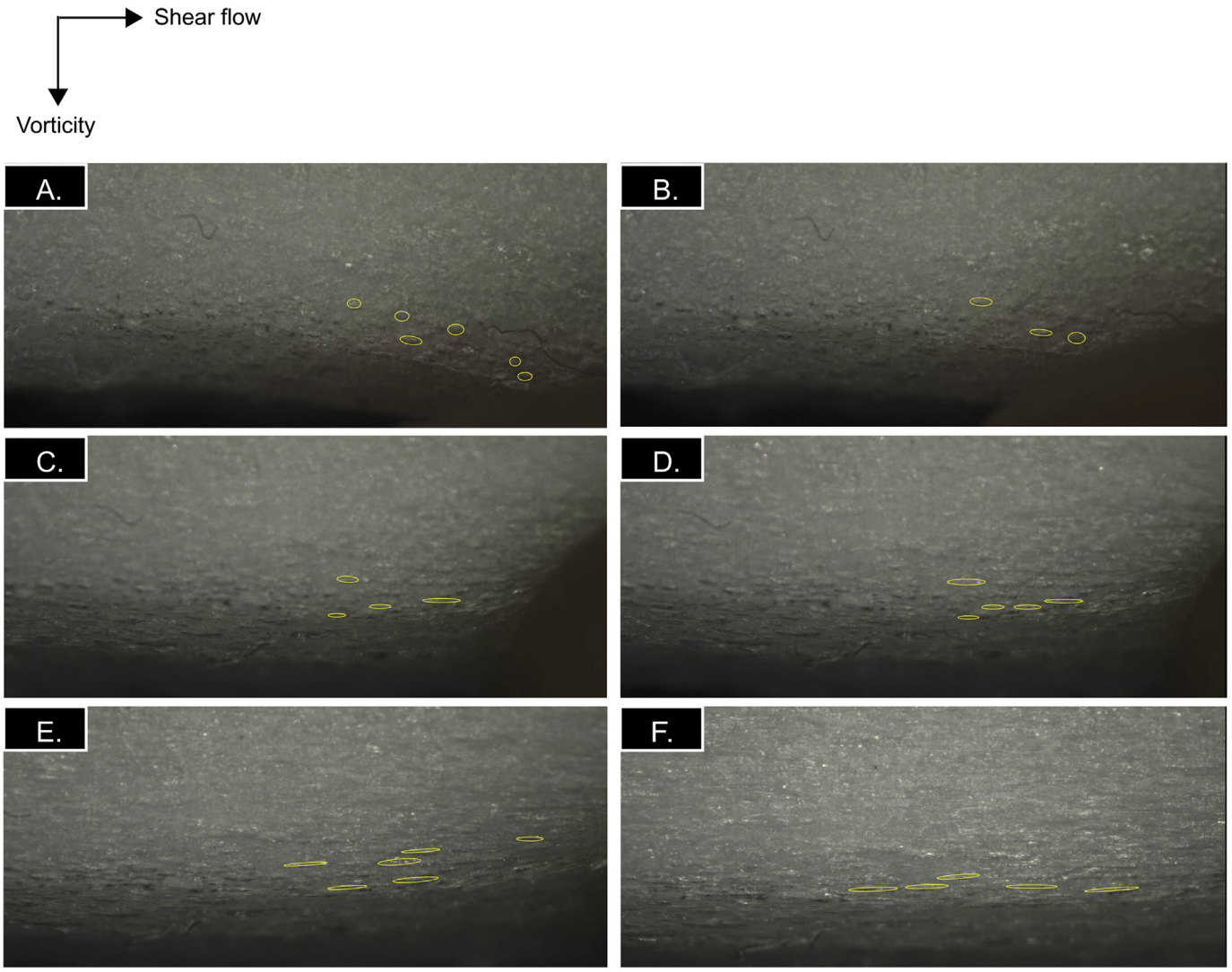

Fig. 8. Morphology changes of air bubbles in a fresh sample (50 rpm, 5 min) when stretched by hand in the parallel direction to shear flow. (A) the bubble deformation before stretching; (B-E) the bubble deformation upon stretching; (F) the bubble formation upon stretching just before breakage. The yellow ellipses have been drawn to sharpen the morphology of bubbles. (For interpretation of the references to colour in this figure legend, the reader is referred to the web version of this article.)

include this effect, Eq. (5) is modified:

$$\sigma_{\parallel} = \sigma_{c\parallel} \bullet (1 - p) \tag{8}$$

As a result, Eq. (7) can be expressed as:

$$AI_{air} = \frac{1 - p}{1 - \left(\frac{a}{b}\right)^{\frac{1}{3}} \bullet p^{\frac{2}{3}}} \tag{9}$$

assuming an isotropic protein phase ($\sigma_{c\parallel} = \sigma_{c\perp}$).The mechanical anisotropy caused by the deformation of air bubbles is plotted as a function of the shear rates applied when making the materials (Fig. 9). Eq. (7) predicts only little anisotropy, given that the bubbles only show limited deformation. However, the bubble deformation during the actual tensile test is much larger, which is illustrated in Fig. 8. If we use the deformations obtained just before breakage (Fig. 8F), the prediction of the mechanical anisotropy is still much lower than what is found with experimental tensile tests.

Fig. 9 depicts the experimental mechanical anisotropy index of fracture stress for the aerated materials and the predicted anisotropy index based on the deformation of air bubbles as a function of the shear rate. Clearly, the deformation of air bubbles does not fully account for the observed mechanical anisotropy. As a consequence, part of the

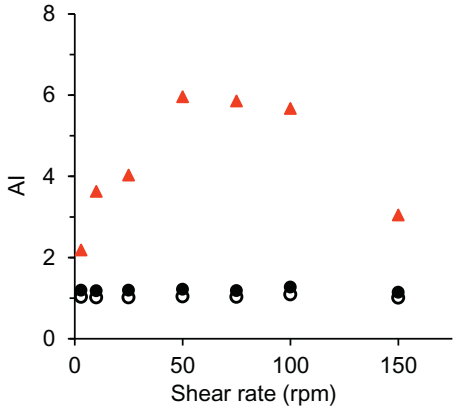

Fig. 9. The experimental mechanical anisotropy index (▲) of fracture stress for the aerated materials at various shear rates (3–150 rpm) for 5 min; the predicted anisotropy index based on the bubble deformation before stretching (○), and the bubble deformation upon stretching just before breakage (●).

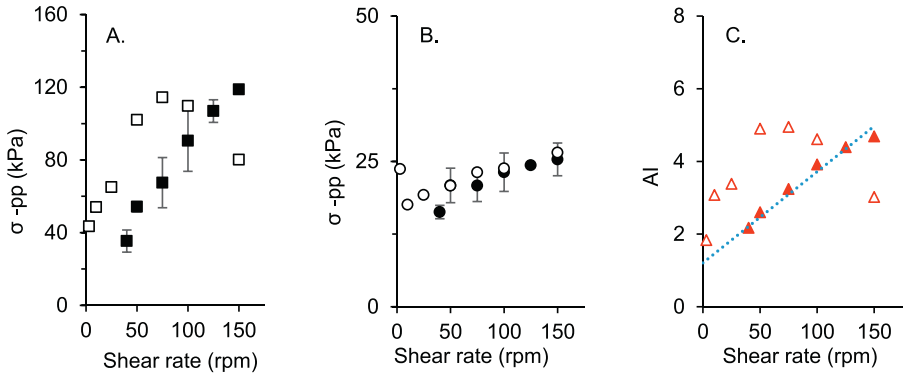

Fig. 10. Comparing experimental (closed symbol) with estimated (open symbol) fracture stress in parallel (A) and perpendicular (B) direction, and anisotropy index (C) of protein phase.

anisotropy must be caused by anisotropy within the protein phase itself. Indeed, a linear relationship between the anisotropy index of deaerated dispersions and shear rate (40–150 rpm) was found (Fig. 7). In addition, we used Eqs. (6) and (8) to estimate the fracture stress of the protein matrix in the aerated materials and compared with the experimental data of deaerated materials (Fig. 10A, B). The estimated data was in good agreement with the experimental data in the perpendicular direction (Fig. 10B). However, the predicted values were higher than the experimental values in the parallel direction. As a result, the experimental anisotropy indices are higher than the experimental values of deaerated material (3–100 rpm) (Fig. 10C). Only the estimation of 150 rpm was much lower than that of 100 rpm. This is thought be due to the breakup of protein alignment in the aerated material. Thus, Eq. (8) is not suitable for the calcium caseinate material with high shear rate (above 100 rpm).

A previous study showed that the fracture stress of aerated material (50 rpm, 5 min) is higher than the material without air in the parallel direction. Our explanation was that air incorporation causes the material to become tougher upon deforming with tensile stress. This factor was taken into account by assuming that air bubbles were infinitely deformed (Eq. (8)). However, the estimated fracture stress in the parallel direction was still higher than the experimented value of the deaerated materials (Fig. 10). This suggests that shearing the aerated dispersion resulted in a stronger protein phase than that in deaerated material. We hypothesis that air bubbles might behave as rigid particles in the protein dispersion during the structuring process, leading to a strengthening of the material. Indeed, non-linear oscillation tests showed that the presence of air bubbles influenced the behavior of calcium caseinate dispersions. The apparent complex modulus of 30% aerated dispersion (137 Pa) was higher than that of deaerated dispersion (39 Pa) with an angular frequency of 10 rad/s and 80% strain. The apparent complex modulus increased to 143 Pa if the deaerated dispersion was whipped with a kitchen mixer to again incorporate air. This effect of air is also supported by several studies on other aerated food (Allen, Murray, & Dickinson, 2008; Chin, Martin, & Campbell, 2005; Tiwari & Bhattacharya, 2011). For example, dairy cream is converted from a viscous liquid into a viscoelastic solid by whipping (Allen et al., 2008). In a study on aeration of elastic fluids, it was shown that the apparent viscosity of the aerated polyacrylamide-corn syrup dispersion is much higher than for ungassed fluids (Cheng & Carreau, 1994). The presence of air bubbles as a rigid dispersed phase will lead to an increase of the local shear rate in the protein phase. This effect will lead to a more anisotropic protein material.

6. Conclusion

The mechanical anisotropy of the fibrous materials was described using a load-bearing model. The void fraction, bubble length and width obtained from X-ray tomography was used to calculate the effect of air bubbles on mechanical anisotropy. Those calculations showed that the deformation of air bubbles could not fully account for the anisotropy of calcium caseinate material. The anisotropy of protein phase plays a greater role on the mechanical anisotropy of the fibrous calcium caseinate material. Therefore, we conclude that the anisotropy of calcium caseinate material is caused by a combination of anisotropy in the protein phase and an additional effect of air.

Supplementary data to this article can be found online at https://doi.org/10.1016/j.foodres.2019.01.009.

Acknowledgements

The authors would like to thank the China Scholarship Council (grant number: 201406820015) for financial support, Friesland Campina for kindly supplying the protein ingredients, Birgit Dekkers for discussions, Remco Hamoen for helping with the X-ray tomography and Jarno Gieteling for technical support.

References

Allen, K. E., Murray, B. S., & Dickinson, E. (2008). Development of a model whipped cream: Effects of emulsion droplet liquid/solid character and added hydrocolloid. *Food Hydrocolloids, 22*(4), 690–699. https://doi.org/10.1016/j.foodhyd.2007.01.017.

Chen, X., Wu, S., & Zhou, J. (2013). Influence of porosity on compressive and tensile strength of cement mortar. *Construction and Building Materials, 40*, 869–874. https://doi.org/10.1016/j.conbuildmat.2012.11.072.

Cheng, J., & Carreau, P. J. (1994). Aerated mixing of viscoelastic fluids with helical ribbons impellers. *Chemical Engineering Science, 49*(12), 1965–1972. https://doi.org/10.1016/0009-2509(94)80080-4.

Chin, N. L., Martin, P. J., & Campbell, G. M. (2005). Dough aeration and rheology: Part 3. Effect of the presence of gas bubbles in bread dough on measured bulk rheology and work input rate. *Journal of the Science of Food and Agriculture, 85*(13), 2203–2212. https://doi.org/10.1002/jsfa.2238.

Cho, K. Y., & Rizvi, S. S. H. (2009). 3D Microstructure of supercritical fluid extrudates. II: Cell anisotropy and the mechanical properties. *Food Research International, 42*(5), 603–611.

Dekkers, B. L., Hamoen, R., Boom, R. M., & van der Goot, A. J. (2018). Understanding fiber formation in a concentrated SPI-pectin blend. *Journal of Food Engineering, 222*, 1–20. https://doi.org/10.1016/j.jfoodeng.2017.11.014.

van der Zalm, E. E. J., Berghout, J. A. M., van der Goot, A. J., & Boom, R. M. (2012). Starch–gluten separation by shearing: Influence of the device geometry. *Chemical Engineering Science, 73*, 421–430. https://doi.org/10.1016/j.ces.2012.02.009.

Gibson, L. J., & Ashby, M. F. (1997). *Cellular solids: Structure and properties* (2nd Ed). Cambridge: Cambridge University Press.

Griffiths, L., Heap, M. J., Xu, T., Chen, C., & Baud, P. (2017). The influence of pore geometry and orientation on the strength and stiffness of porous rock. *Journal of Structural Geology, 96*, 149–160. https://doi.org/10.1016/j.jsg.2017.02.006.

Hoek, A. C., Luning, P. A., Weijzen, P., Engels, W., Kok, F. J., & de Graaf, C. (2011). Replacement of meat by meat substitutes. A survey on person- and product-related factors in consumer acceptance. *Appetite, 56*(3), 662–673. https://doi.org/10.1016/j.appet.2011.02.001.

Hyun, S. K., Murakami, K., & Nakajima, H. (2001). Anisotropic mechanical properties of porous copper fabricated by unidirectional solidification. *Materials Science and Engineering, 299*(1), 241–248.

Ji, S., Gu, Q., & Xia, B. (2006). Porosity dependence of mechanical properties of solid

materials. *Journal of Materials Science, 41*(6), 1757–1768. https://doi.org/10.1007/s10853-006-2871-9.

Manski, J. M., van der Goot, A. J., & Boom, R. M. (2007). Formation of fibrous materials from dense calcium caseinate dispersions. *Biomacromolecules, 8*(4), 1271–1279.

Manski, J. M., van der Zalm, E. E. J., van der Goot, A. J., & Boom, R. M. (2008). Influence of process parameters on formation of fibrous materials from dense calcium caseinate dispersions and fat. *Food Hydrocolloids, 22*(4), 587–600.

Manski, J. M., van Riemsdijk, L. E., Boom, R. M., & van der Goot, A. J. (2007). Importance of intrinsic properties of dense caseinate dispersions for structure formation. *Biomacromolecules, 8*(11), 3540–3547.

Masmoudi, M., Kaddouri, W., Kanit, T., Madani, S., Ramtani, S., & Imad, A. (2017). Modeling of the effect of the void shape on effective ultimate tensile strength of porous materials: Numerical homogenization versus experimental results. *International Journal of Mechanical Sciences, 130*(June), 497–507. https://doi.org/10.1016/j.ijmecsci.2017.06.011.

Nakajima, H. (2007). Fabrication, properties and application of porous metals with directional pores. *Progress in Materials Science, 52*(7), 1091–1173. https://doi.org/10.1016/j.pmatsci.2006.09.001.

Rice, R. W. (1993). Comparison of stress concentration versus minimum solid area based mechanical property-porosity relations. *Journal of Materials Science, 28*, 2187–2190.

Rice, R. W. (1996a). Evaluation and extension of physical property-porosity models based on minimum solid area. *Journal of Materials Science, 31*, 102–118.

Rice, R. W. (1996b). The porosity dependence of physical properties of materials: A summary review. *Key Engineering Materials, 115*, 1–20. https://doi.org/10.4028/www.scientific.net/KEM.115.1.

Tian, B., Wang, Z., van der Goot, A. J., & Bouwman, W. G. (2018). Air bubbles in fibrous caseinate gels investigated by neutron refraction, X-ray tomography and refractive microscope. *Food Hydrocolloids, 83*, 287. https://doi.org/10.1016/j.foodhyd.2018.05.006.

Tiwari, S., & Bhattacharya, S. (2011). Aeration of model gels: Rheological characteristics of gellan and agar gels. *Journal of Food Engineering, 107*(1), 134–139. https://doi.org/10.1016/j.jfoodeng.2011.05.036.

Wang, Z., Tian, B., Boom, R., & van der Goot, A. J. (2019). Air bubbles in calcium caseinate fibrous material enhances anisotropy. *Food Hydrocolloids, 87*, 497–505. https://doi.org/10.1016/j.foodhyd.2018.08.037.